NAL PROPOSAL No. 219

Scientific Spokesman:

P. Oddone
Lawrence Berkeley Laboratory
University of California
Berkeley, California 94720

FTS/Comm: 415 843-2740 X 5367

DETAILED STUDY OF NUCLEON DISSOCIATION AND PARTICLE EXCHANGE REACTIONS

R. Birge, R. Ely, G. Gidal, D. Grether and P. Oddone

Lawrence Berkeley Laboratory

May 25, 1973

DETAILED STUDY OF NUCLEON DISSOCIATION AND PARTICLE EXCHANGE REACTIONS

R. Birge, R. Ely, G. Gidal, D. Grether, and P. Oddone

Lawrence Berkeley Laboratory
University of California
Berkeley, California 94720

ABSTRACT

We propose to study the reaction

$$\pi^- p \longrightarrow \begin{matrix} \pi \\ k \\ p_{fast} \end{matrix} + x$$

at 50 and 100 GeV over a wide range of momentum transfers and recoiling masses. We will use a streamer chamber to study the components of x and a magnetic spectrometer to measure the fast outgoing track. We will be able to investigate nucleon diffraction with sufficient resolution to study the resonances, and we will obtain information on particle exchange reactions. The apparatus has been designed so that the experiment can be extended to study different incident and outgoing particles in the energy range from 50 to 200 GeV.

Date: May 25, 1973

Scientific Spokesman:
P. Oddone

TABLE OF CONTENTS

		Page
I.	INTRODUCTION	1
II.	PHYSICS	3
	A. Diffraction	3
	B. Higher Missing Mass	6
	C. Particle Exchange Cross Section	6
	D. Possible Future Extensions	7
III.	EXPERIMENTAL DESIGN	9
	A. General Layout of the Experiment	9
	B. The Triggering Scheme	11
	C. Resolution During Triggering and During Analysis	17
	D. Momentum Transfer and Mass Acceptance	20
	E. Triggering Rates	22
	F. Cerenkov Counters	25
	G. Beam	25
	H. Comparison With Other Experiments	26
IV.	IMPLEMENTATION	27
	A. Personnel	27
	B. Equipment and Costs	27
	C. Machine Time Requirements	28
V.	REFERENCES AND FIGURES	30

I. INTRODUCTION

We propose to study the reaction

$$\pi^- + p \rightarrow \begin{matrix} \pi \\ k \\ p \end{matrix}_{\text{fast}} + X$$

in the incident energy range from 50 to 100 GeV, and over a wide range of momentum transfers t and masses M_X of X. In particular, we will study nucleon diffraction dissociation with sufficient resolution to observe the resonances and do reconstruction with one neutral particle in the final state (1 constraint fits). As a by-product we will obtain information on particle exchange reactions where the outgoing fast particle is different from the incident particle.

We will use a streamer chamber to observe the fragments of X and a small-aperture-medium-resolution spectrometer to observe the forward scattered particle. The streamer chamber will be triggered when the momentum of the outgoing fast particle, as observed in the spectrometer, implies that the X recoil has a mass and momentum transfer within a specified range.

The streamer chamber will be of conventional design, dictated by the magnet that NAL would make available.

The spectrometer design is governed by two rules: (a) a large enough aperture to run the experiment efficiently; and (b) a resolution sufficiently good to eliminate proton recoils (elastic scattering) during the trigger and allow 1C fits during reconstruction. These criteria lead to a design with two consecutive bending magnets some 20 m. downstream from the streamer chamber with a total integrated field 80 kg. m. Apertures for the magnets of 20 by 40 cm. seem ideal, but apertures down to one fourth the area are still adequate to carry out the experiment.

Proportional wire chambers placed in the spectrometer will detect the fast scattered particle. The decoding of the proportional chambers, fitting of the particle track, and calculation of the momentum and momentum transfer will be done by a simple hard-wired calculator which will perform the arithmetic in less than one microsecond. The streamer chamber will be triggered on the result of the calculation.

The addition of Cerenkov counters will allow the separation of forward scattered protons, pions and kaons in the kinematic regions where a substantial admixture of these particles exists.

We intend a first run with incident π^- beam of some 5×10^5 machine pulses. This run would be divided between 50 GeV and 100 GeV, and produce about 5×10^5 events. The experiment can be extended to 200 GeV, but this involves doubling the magnitude of the spectrometer field integral. We prefer to gain some experience at 50 GeV and 100 GeV before extending the experiment to 200 GeV.

Our proposed experiment has advantages over other experiments, including bubble chamber and spectrometer experiments, for studying in detail diffraction dissociation and various exchange reactions. We describe these advantages in Section IIIH.

Our large facilities at Berkeley should allow us to analyze the experiment quickly. All our analysis programs, originating from our streamer chamber work at the Bevatron and our triggered diffraction bubble chamber experiment at SLAC, should be ready well in advance of our data taking.

II. PHYSICS

A broad class of reactions can be studied with the apparatus we propose.

A. Diffraction

The primary goal of this experiment is to study in detail diffractive nucleon dissociation. The motivation for studying nucleon dissociation arises both from experiments at pre-NAL accelerator energies and recent experiments at the ISR.

Experiments below 10 GeV show low mass enhancements in the mass spectrum of the dissociated nucleon. The early missing mass experiments showed the existence of these enhancements conclusively.[1] Later work, especially using bubble chambers, concentrated on studying the detailed composition and spin parity properties of the mass spectrum.[2] All published experiments lack the statistics necessary to perform the required partial wave analysis, however. The association of these enhancements with known resonances thus remains a controversial subject.

Two experiments being analyzed should go a long way in helping to understand the composition of the mass spectrum. One is our experiment $\pi^{\pm}p \rightarrow \pi^{\pm} N^*$ at 14 GeV (Caltech-Berkeley-SLAC collaboration) using the 40-inch bubble chamber with a downstream spectrometer.[3] The memory time of the bubble chamber (~2 milliseconds) is used to make a software decision based on track reconstruction with a Sigma 2 computer. The sample of events obtained is approximately 10^5 N^* for each sign of the incident beam in the region of mass enhancements. The experiment is limited in that dead areas for the beam restrict the study of very small momentum transfer events ($-t$ less than .02 $(GeV/c)^2$) while the

steep t dependence ($d\sigma/dt \sim e^{+8t}$) limits severely the number of events above $-t \approx .3\ (GeV/c)^2$.

The second experiment is the Bookhaven Spectrometer experiment which studies p + Nucleus → p^* + Nucleus.[4] Events coherently produced are selected and thus limited to a very small t range. Presumably coherent scattering reduces the background due to exchanges other than Pomeron.

Both experiment described above will have sufficient statistics to attempt a partial wave decomposition of the final state. The importance of performing such an analysis has been demonstrated by the CERN-I HEP collaboration in the case of pion dissociation.[5]

Nucleon dissociation studies will be useful, given the many known resonances that can be produced diffractively. Our proposed experiment extends the study of these mass enhancements to NAL energies where diffraction events should be freer from non-diffractive backgrounds. Our experiment extends the detailed study of the mass spectrum to considerably larger t (from 0 to -1.5 $(GeV/c)^2$) and over a wide range of s; it has the ability to do 1C and 4C fits, and to study the strange particle decay of the enhancements.

Perhaps the most important incentive for studying nucleon diffraction is provided by the recent ISR results of the Aachen-CERN-Harvard-Geneva-Torino and the CERN-Holland-Lancaster-Manchester collaborations.[6] Contrary to some expectations they observe that the diffractive bump in the mass spectrum extends to masses of almost 10 GeV at the highest ISR energies. These higher mass excitations were found to be associated with higher multiplicities, a result which has been confirmed by the NAL bubble chamber experiments.[7] Although their mass resolution is quite poor, due largely to the ISR machine characteristics, they have evidence for

scaling of the diffractive bump. If the invariant cross section $s \frac{d\sigma}{dtd M_x^2}$ is independent of s, then M_x^2/s is the scaling variable, and the diffractive bump of width ΔM scales as $\Delta M_x^2/s$. The ISR experiments are then consistent with the following table:

P_{lab}(GeV)	20	50	100	200	1500
s(GeV^2)	40	100	200	400	2500
ΔM(GeV)	1	1.6	2.2	3.2	~8

Thus NAL energies more than double the mass interval of nucleon excitation previously available at pre-NAL accelerator energies. The momentum transfer dependence of the diffraction peak, while comparable to elastic scattering at small t, becomes shallower at intermediate t values ($d\sigma/dt \sim e^{+4t}$ above $-t = .5$ (GeV/c)^2). Our apparatus will allow us to study this increased mass range in detail. We will be able to undertake the following program:

(a) A partial wave analysis to look for new resonances in the various decay channels and to study possible spin alignment rules as a function of t and M_x;

(b) A study of the multiplicity and strange particle production as a function of t and M_x;

(c) Detailed comparisons with incident p, π, k to test factorization for any given region of M_x and to a t of ~ 1 GeV^2;

(d) A study of the energy dependence up to 200 GeV;

(e) Study of final state momenta distribution for large masses M_x.

B. Higher Missing Mass (Triple Regge Limit)

We will be able to look at masses beyond the diffraction peak and ask similar questions to those we will ask of the diffraction bump. The triple Regge formalism may allow comparisons between Pomeron or Reggeon-nucleon scattering and Particle-nucleon scattering. We will attempt kinematic fitting, study multiplicities and strange particle production as a function of t and M^2, look at momenta distribution of the target fragments, and make comparisons for various projectiles.

C. Particle Exchange Reactions

The apparatus we propose is suited to the study of the reactions

$$\pi+p \rightarrow K+X,\ p+X$$
$$K+p \rightarrow \pi+X,\ p+X$$
$$p+p \rightarrow K+X,\ \pi+X$$

involving particle exchanges. The study of these exclusive channels should complement the investigation of the inclusive cross section with the focusing spectrometer at NAL.[8] In particular, one could study the multiplicity as a function of mass, strange particle production, and differences as a function of t. Again, for these channels one would be able to do 1C and 4C fits.

Consider, for example, the case of baryon exchange (Δ) in the reaction

$$\pi^- p \rightarrow p + X$$

This is certainly one of the smallest particle exchange cross sections in the region of the resonances ($X = \rho$, A_1, A_2). It has been studied in

missing mass experiments, but there is no published data on the final state X. There is one experiment presently being analyzed by the Illinois-Argonne group at 8 GeV which uses the Argonne streamer chamber to look at the components of X. Two more experiments are planned: our streamer chamber experiment at the Bevatron at 4 GeV and the CERN Ω-Spectrometer experiment up to 16 GeV, both likely to run in the Fall, 1973.

We can estimate the cross section at 50 GeV by extrapolating the inclusive cross sections observed at 16 GeV.[9] We obtain a total cross section $\pi^- p \to p + X$ in the region of X masses from 0 to 1.4 GeV of ~ 0.16μb at 50 GeV. With the downstream spectrometer set in the forward direction we would obtain ~3500 events running the streamer chamber at a luminosity of 10^{30} cm^{-2} $pulse^{-1}$ for 100 hours. This is probably not the experiment in which to study in great detail the decay distributions of the low mass resonances, ρ, A_1, A_2, produced in the backward direction. It is much easier at lower energies. But, by being able to study the 1C and 4C fits, we should be able to have a clean experiment to determine cross sections and to some extent partial waves and t dependences. The cross section for large mass X, on the other hand, increases rapidly as a function of M_X (approximately as the cube of the mass[10]), and for $M_X > 3$ GeV the cross sections are large enough for detailed study.

D. Possible Future Extensions

A streamer chamber at NAL would be desirable as a general research tool; many experiments after ours can be done with relatively short preparation times. The development of a selective trigger as we propose would allow us to select any particular anomaly or surprise discovered by the missing mass experiments and to study it in detail.

The addition of a γ detector would allow the study of the charge exchange reaction

$$\pi^- p \rightarrow \pi^0 + X.$$

Another possible experiment is the study of large perpendicular momentum events. The unexpectedly large cross sections observed at ISR, possibly due to yet unexplained scattering processes, provide incentive for the study of these events. A variety of triggers for large perpendicular momentum events is possible, some involving calorimeters at large angles and others using the dispersion of the streamer chamber magnet coupled with track reconstruction in a fast calculator to find an approximate momentum.

III. EXPERIMENTAL DESIGN

A. General Layout of the Experiment

Aperture considerations (Section IIID) and resolution considerations (Section IIIC) lead to the design shown in Figure 1. The streamer chamber contains a 45 cm. H_2 target and is placed in a magnet with a total integrated field of 30 kg.m. The streamer chamber size will depend on the available magnet and thus the parameters described for it are only tentative. Immediately following the streamer chamber there is a small bending magnet whose function is to cancel the dispersion introduced by the streamer chamber magnet. Its aperture can be quite small (5 cm. gap x 10 cm. wide) and it should have 20 kg.m. integrated field. We have considered designs without the compensating magnet and found them adequate provided the experiment is to run efficiently for only one charge of the outgoing track. In order to run both positive and negative particles simultaneously with a similar momentum transfer acceptance the compensating magnet is necessary.

Downstream from the streamer chamber and the compensating magnet are two proportional wire chamber stations which measure the outgoing angle. Between these two stations lie two threshold Cerenkov counters to distinguish π, k, p up to 100 GeV/c.

A spectrometer magnet of small aperture (20 cm. gap x 40 cm. wide) follows with an integrated field of 80 kg.m. This field is adequate up to 100 GeV, but should be doubled for operation of the experiment at 200 GeV.

Downstream from the spectrometer magnet there are two more proportional wire chambers to determine the angle after the bend. In order to trigger on both positive and negative particles simultaneously, the last

station is split into two legs: one along the axis for the positive particles and one along the axis for the negative particles. The separation of positive and negative particles at the last station is approximatley 2.3 meters at 50 GeV. In the remaining discussions we consider only one leg, the second being logically identical to the first.

The proportional wire chamber stations will consist of an x and y coordinate at each station, with 1 mm. wire spacing, and a drift chamber in the y coordinate. The 1 mm. proportional wire chambers will be used both during the trigger calculations and during the analysis. The drift chambers with a resolution $\sigma = 125\mu$ will be used only during the analysis and will permit a more accurate determination of the bend angle.

Table I shows the proportional chamber sizes and number of wires. The number in parenthesis indicates those chambers which need not be included in the trigger logic.

	y	x
STATION 1	5 cm 50 wires	3 cm 30 wires
STATION 2	40 cm 400 wires	20 cm 200 wires
STATION 3	40 cm 400 wires	(20 cm) (200 wires)
STATION 4	100 cm 1000 wires	(40 cm) (400 wires)
TOTAL WIRES	1850 wires	830 wires

Table 1: Station sizes and number of wires. Numbers in parentheses are those not used in the trigger. The bend is in the yz plane.

In the sections that follow, let the beam be incident along the z direction and the plane where the bends take place by the yz plane. Let the subscripts a,b,c,x represent the incident, target, fast triggered and recoil particles, respectively. Also, let p, E, and t denote momentum, energy, and momentum transfer.

B. The Triggering Scheme

Since we are using optical techniques to study the final state, it is important that a large fraction of the pictures taken contain an interesting event. Thus a trigger with high efficiency must be established.

We have used as a model for our trigger the triggering scheme of our bubble chamber experiment at SLAC. We find in our SLAC experiment that ~50% of the pictures contain a trigger-selected event. The remaining 50% of the triggers arise to a large extent from: a) interactions in the bubble chamber entry and exit windows; b) interactions in the invisible portions of liquid hydrogen; and c) muon contamination in the beam.

The trigger in our SLAC experiment makes a reconstruction only in the plane where the bend occurs (the yz plane). The triggering we propose here contains also a partial reconstruction in the plane perpendicular to the bend plane (the xz plane). This additional requirement should make the fraction of useful events higher than in our SLAC experiment since it helps in discriminating muons. The absence of high pressure windows, and invisible areas of hydrogen, should also help in obtaining a higher fraction of useful pictures.

The instantaneous beam rates that we plane to use (~250K particles per spill) are about 1/40 of the instantaneous rates of the SLAC

experiment. Thus we feel no uncertainty in extrapolating our present experience to the domain of this proposal.

The trigger we propose is in a sense equivalent to a complete analysis of a missing mass experiment carried out at a rate of 10^6 events per second.

The requirements we plan to impose for triggering are the following:

1. No double hits in any of the proportional chambers (a double hit on two adjacent wires is considered a single hit at the average position of the two wires).
2. The track found in the x-z and in the y-z planes must extrapolate to the intersection of the beam and target.
3. The track in the y-z plane found in the first two stations must match the track found in the last two stations when extrapolated to the middle of the spectrometer magnet.
4. The recoil mass implied by the track,

$$m_x^2 = m_{proton}^2 + 2mp(E_a - E_c) + t \,,$$

must be within the specified limits. As we will discuss in more detail later, the energy difference $(E_a - E_c)$ is approximated by the momentum difference $(p_a - p_c)$, and the momentum transfer t is approximated by the perpendicular momentum squared.

5. The proper Cerenkov counter configuration will be required.
6. A t cut may be placed if the t range under exploration needs to be narrowed more than the range provided by the geometrical

acceptance of the spectrometer. This is generally not needed.

The design of the calculating unit is greatly simplified by the requirement that there be only one hit per station and by using the strategic distance ratios of the apparatus layout shown in Figure 1.

The unit which we will sketch is one of several fast logic schemes one may use. Our interest in giving details is to demonstrate the relative ease with which complicated fast logic decisions may be made using available technology.

While streamer chambers have long memory times, ion diffusion causes a rapid increase of the measuring error as a function of the triggering delay time. Figure 2 shows the growth of the measuring error as a function of delay time. From Figure 2 and the requirement of not compromising our ability to do 1C fits, we conclude that we need to trigger the streamer chamber within 2 μsec.

Figure 3 shows the general scheme of the electronics at whose core lies the arithmetic unit. The column on the left of Figure 3 shows the cumulative time required by the various stages. Below we describe each component in detail.

a. Amplification and pulse shaping

We plan to use conventional circuits well tried at SLAC and LBL.[11] Figure 4A shows a sketch of this part with an input amplifier stage and a pulse shaper at the output to produce 50 nsec pulses. The propagation time for this circuit is < 50 nsec. We allow 100 nsec.

b. Delay stage

This stage is associated with the necessary cables to carry the information to the decoding and calculating units. The delays are

non-trivial since our apparatus is some fifty meters long. If we assume a propagation of signals at 2/3 speed of light, then placing the calculating units 5/6 the length of the apparatus downstream from the streamer chamber will make the signals from the streamer chamber area and the area of station 4 arrive simultaneously, in approximately 300 nsec. The timing could be improved by using faster cables or by decoding locally at each station and then sending the results over faster cables.

c. Write/Read latches

Again quite conventional design will be used as shown in Figure 4B. The latches are set (written) by a fast signal strobe such as might be generated by a beam counter or a coincidence of a Cerenkov and beam counter. The function of the latches is to stabilize the levels which will serve as input to an asynchronous computing unit. A second function of the latches is to allow the reading of these levels into a computer interface after the picture is taken (whenever a read strobe is pulsed). We have assumed here a conservative 50 nsec for the propagation time through the latches.

d. Decoding of adjacent hits

This is simply done by generating intermediate signals for those sets of wires which have adjacent hits. Figure 4C shows the input wires as being the even number sequences and the output signals containing, in addition, the odd wire sequence (adjacent hits). A 50 nsec propagation is assumed.

e. Encoding of the coordinates

After having encoded adjacent hits we have doubled the number of signals. These signals are then encoded into an eleven bit binary number using a diode matrix as illustrated in Figure 4D. We estimate less than 50 nsec encoding time. The numbers are encoded in such a way that they all

measure distance from a point located at a fixed distance from the axis of the apparatus. If we use the large aperture magnet with a 20 cm x 40 cm. gap, then the largest chamber, located at station 4, is 100 cm. across. After decoding of the adjacent hits this leaves us with a possible maximum distance of 2000 (1/2 mm. least count).

f. The arithmetic unit

In what follows let x_i, y_i represent the coordinates at station i. For each addition and subtraction we have allowed 100 nsec. This time is quite abundant, using modern integrated circuits with propagation times less than 10 nsec for 4 bit arithmetic. In calculating the momentum transfer we use 4 x 4 bit multipication, and this is carried out by simply addressing a read only memory with the higher 4 bits of the numbers being multiplied. Again, for this type of operation we assume 100 nsec propagation time, although less than 50 nsec might be more realistic.

The operations to be carried out are shown below. The results of the operations appearing on the right hand side are fed to a comparator stage (see Figure 3) which generates the trigger if all results are within limits.

-Extrapolation to the target:

$$x_1 - \frac{(x_2-x_1)}{8} = \text{xTARGET} \qquad \text{(i)}$$

$$y_1 - \frac{(y_2-y_1)}{8} = \text{yTARGET} \qquad \text{(ii)}$$

-Match at the midpoint of the spectrometer:

$$y_2 + \left(\frac{y_2-y_1}{8}\right) - y_3 + \left(\frac{y_4-y_3}{8}\right) = \text{MATCH} \qquad \text{(iii)}$$

-Bend angle calculation (expressed in wire counts):

$$(y_4-y_3) - (Y_2-y_1) = \text{BENDY} \quad \text{(iv)}$$

-Momentum transfer calculation:

Because the momentum transfer is dependent on the measured spectrometer momentum, it cannot be calculated exactly before the result of the bend angle calculation is ready. Instead we approximate the momentum by

$$-t = P_a^2 \, \theta^2 \qquad \text{(v)}$$

where θ^2 is measured by the coordinate at station 2, namely by

$$\text{TAPRX} = c \; \{(x-x_{BEAM})^2 + (y-y_{BEAM})^2\} \qquad \text{(vi)}$$

where C translates this measurement into units that allow one directly to combine t with BENDY in calculating the recoiling mass. xBEAM and yBEAM are the projected coordinates of the beam at station 2 using a proportional chamber upstream of the streamer chamber. There is a one to one correspondence between points in the beam chamber and the position at station 2 if one assumes a point target. Notice that the t approximation (v) is good in the neighborhood of elastic scattering (Figure 5), deviating slowly for larger recoiling masses. Also note that the dispersion at station 2 gives non unique values for the momentum transfer. The effect is small due to the compensator magnet which cancels the average dispersion of the streamer chamber magnet. The remnant dispersion is due to the target size and is shown in Figure 10C.

-Recoiling mass calculation:

The recoiling mass is given by

$$M_x^2 = m_{proton}^2 - 2m_{proton}\,(E_a - E_c) + t \qquad \text{(vii)}$$

This can be transformed to

$$M_x^2 - m_p^2/2mp = (E_a - E_c) + t/mp$$

and the triggering limits placed on the quantity at the right of the equation. With our approximations this translates into

$$(x_4 - x_3) - (x_2 - x_1) + c\,\{(x - x_{BEAM})^2 + (y - y_{BEAM})^2\} = \text{MASS} \qquad \text{(viii)}$$

Figure 6 shows the arithmetic unit and the timings necessary to carry out all the operations. Notice that x/8 denotes that the number x is shifted three bits when added to another number. The total time as shown is .5 μsec for the calculations.

g. Detection of non adjacent hits

The event is vetoed if any chamber is empty or if it has more than one hit. This detection is done immediately after encoding the adjacent hits. It is carried out in parallel to the operations of the arithmetic unit. All wire signals are added via resistors to a common link. The current flow in the link is required to be equivalent to only one wire hit (Figure 4E).

C. Resolution

To avoid confusion we define two missing masses: one which we will simply call the missing mass, is the mass of the object X in the reaction

$$a + b \rightarrow c + X$$
$$\quad\quad\quad\quad\quad\quad\quad\quad \hookrightarrow \text{charged + neutral tracks;}$$

the second we will call the neutral missing mass, and it is the mass of the undetected neutrals. In this section we will describe the resolution for these two missing masses.

In the missing mass of X, given by

$$M_x^2 = m_p{}^2 + 2mp\ (E_a - E_c) + t,$$

the error enters essentially in the measurement of $(E_a - E_c)$. The errors in t are negligible because we measure angles very well. The contributing errors to $(E_a - E_c)$ arise from the beam momentum uncertainty ΔP_a, and the error in the momentum of the outgoing track ΔP_c. We have

$$\Delta M_x^2 = 2m\ \Delta E = 2m\ \Delta P,$$

where

$$\Delta P = \sqrt{\Delta P_a^2 + \Delta P_c^2} \quad .$$

Since the momentum P_c is measured by the bend angle θ, the error P_c is given by

$$\Delta P_c \leq \frac{\Delta\theta}{\theta_a} P_a \ ,$$

where θ_a is the bend angle of the beam. This error corresponds to the error in the largest possible momentum and thus is an overestimate of the error for $M_x > m_p$. For a given fixed spectrometer field integral the bend angle θ_a is inversely proportional to P_a, making the error ΔP_c proportional to the square of the incident momentum in an apparatus where the error is dominated by chamber resolution. This is the main experimental problem in extending the experiment to high energies. The fact that multiple scattering decreases as the energy increases ameliorates the steep dependence on the incident beam momentum. In the limit in which errors are dominated by

multiple scattering the dependence of Δp_c is linear in p_a.

In calculating $\Delta\theta$ we consider the measurement errors due to the finite wire spacings and the effects of all discrete and continuous sources of multiple scattering. We display the results in Table II, where we have chosen to display the effects of multiple scattering as an increased measurement error at stations 1 and 4. In addition we display the results of a similar calculation for our SLAC spectrometer at 14 GeV/c. From Table II we conclude that the resolution for the proposed experiment is better at 50 GeV, and only slightly worse at 100 GeV, than the resolution of our SLAC experiment at 14 GeV/c. We observe also from Table II that the resolution during analysis at 100 GeV is limited by multiple scattering. Thus if better resolution drift chambers are used ($2\sigma \simeq 160\mu$) and the field integral is doubled, we could run the experiment at 200 GeV with similar resolution.

Resolution 2σ(mm)	50 GeV (Proposed)		100 GeV (Proposed)		14 GeV (Confirmed)
	Trigger	Analysis	Trigger	Analysis	Trigger = Analysis
Station 1	1.29	.84	1.1	.47	.75
Station 2	1.0	.250	1.0	.250	.66
Station 3	1.0	.250	1.0	.250	.66
Station 4	1.33	.9	1.1	.45	1.65
$\Delta P_c(2\sigma)$ MeV	100	55	361	129	112
ΔP_{BEAM} (2σ) MeV	50.0	50	100	100	70
ΔP TOTAL $\approx \Delta M$ 2σ MeV	112	74	374	163	138

TABLE II. Comparisons of resolution at 50 and 100 GeV. Multiple scattering is shown as an increased point setting error in stations 1 and 4.

The resolution of the apparatus is such that we will be able to reduce substantially the elastic triggers. To see this consider a cut on the missing mass at 1.2 GeV/c. Then the trigger must separate $m_p^2 = .86\ (\mathrm{GeV})^2$ from $M^2_{CUT} = 1.44\ (\mathrm{GeV/c})^2$. With a resolution of $\sigma(2m_p\Delta p) = .112\ \mathrm{GeV}^2$ we see the elastic peak and the cut are separated by approximately 5 standard deviations.

The neutral missing mass resolution is determined to a large extent by the resolution in the missing mass M_X. We have investigated this resolution and have concluded that our resolution in the neutral missing mass will be comparable, and in some cases better, than the resolution in our 14 GeV experiment. The resolution at 14 GeV is shown in Figures 7 and 8 for the π^o and neutron peaks respectively. Figure 9 shows that the fits to the π^o and neutron hypothesis can be separated most of the time without use of ionization information.

The measurement of slow tracks < 1 GeV in the bubble chamber are limited by multiple scattering errors. The streamer chamber has a point setting error about 3 times that of the bubble chamber. The absence of significant multiple scattering leads us to expect slightly better overall resolution.

D. Momentum Transfer and Mass Acceptance

The accept ance of the apparatus is predominantly determined by the spectrometer magnet aperture.

To understand qualitatively the acceptance, we show the position of the scattered particle at the entrance of the spectrometer magnet in Figure 10A. A given recoiling mass M_X and momentum transfer t specify a fixed scattering angle. Thus events of fixed M_X and t appear as circles

in the entry plane of the magnet. The radius of the circle grows approximately as $\sqrt{t}$ and is roughly independent of the recoil mass as shown in Figure 10B. In the absence of a compensating magnet the origin of the circles is displaced as higher masses M_X are produced (lower outgoing momenta), as shown in Figure 10C. With the compensating magnet all masses have the same origin within the spread introduced by the finite target length.

In calculating the acceptances we have assumed the station sizes shown in Table I.

Figure 11 shows the t acceptance for a mass M_X of 2 GeV at 50 GeV for three positions of the spectrometer relative to the beam. We see generally that when the spectrometer is centered on the beam the t acceptance is very narrow. As the aperture is displaced from the beam position, the t acceptance becomes quite smooth, however.

Figures 12 and 13 show examples of the acceptance for several missing masses as the spectrometer is displaced up to 0.5 meter from the beam position. The conclusions from the acceptance calculations are:

a) The t acceptance is only weakly dependent on the recoiling mass.

b) The acceptance for various momentum transfer bites are quite smooth within the limits accepted, and of adequate size.

c) The best mode of operation consists in displacing the spectrometer relative to the beam along the x direction (laterally if we chose the plane of bends to be the vertical plane). For any given position a momentum transfer bite is selected which varies only slowly according to the mass M_X.

d) Outgoing positive and negative particles may be run simultaneously.

E. Trigger Rates

The streamer chamber memory time can be made as small as 2 μsec. Using this memory time, the flux limitations for the streamer chamber can be set by either of the following two criteria: 1) on the average one should have less than one beam track in addition to the track which interacts; and 2) on the average one should have less than one additional interaction. The first criterion leads to a flux limitation of ~2.5×10^5 particles per pulse corresponding to a luminosity of $4 \times 10^{+30}$ cm^{-2} $pulse^{-1}$. The second criterion leads to a flux limitation of 7×10^6 particles per pulse corresponding to a luminosity of 7×10^{30} cm^{-2} $pulse^{-1}$. From the analysis point of view we prefer to run the experiment using criterion 1) except in the limited runs in which we would study very rare events. Beam-bunching will reduce the maximum tolerable fluxes.

The calculating unit places restrictions on the flux when the beam passes through the proportional chambers (e.g. when studying low momentum transfer events). Since the unit operates at a megacycle we estimate again a likely limitation of 2.5×10^5 particles per pulse. When the proportional chambers are displaced outside of the beam area then the maximum beam rates are set by the streamer chamber only.

In practice when studying events with large cross sections the limitation in the data taking rate is placed by the streamer chamber camera recycling time. We expect to approach a capacity of 4 pictures per machine pulse. The event rates for diffraction excitation are such as to permit the study of the diffractive bump up to $-t \approx 2$ $(GeV/c)^2$. Table III shows the estimated rates for the diffraction bump for various spectrometer settings. We have used the observed differential cross

sections of the CERN-Holland-Lancaster-Manchester (CHLM) collaboration shown in Figure 16. The numbers are only approximate and intended to show the regions where significant numbers of events may be obtained. We have fitted the differential cross section for the bump with a form $d\sigma/dt = 2oe^{+5.3t}$ .mb/(GeV/c)^2 which is the average behavior between t = 0 and -t = 1.0(GeV/c)^2. The slope observed at smaller -t is sharper than that observed at large -t making our estimate of rates for -t > 1.0 (GeV/c)^2 somewhat low. The apparatus acceptance has been folded in, and its approximate values indicated in the table.

In Table III we also show the event rates for large missing mass estimated from the CHLM collaboration results. The numbers shown are per 1 GeV^2 interval in M_X^2.

The particle exchange cross sections in the region of large M_X^2 ($M_X^2 \gtrsim 9$) are about an order of magnitude smaller than the cross sections for events with a leading particle identical to the beam.[12] They are adequate for detailed study.

In the region of small missing masses the rates are smaller. To set limits on the experiment we have considered the reaction $\pi^- p \to p + X$ and integrated the cross section from $X = \pi^-$ to $X = A_2$. We have used the data at 16 GeV and extrapolated it using $\sigma_T \propto \frac{1}{p^{2.5}}$. The estimated rates are also shown in Table III. Since the cross section increases rapidly with the mass M_X the rates are satisfactory for large M_X.[10]

Spectrometer setting		Beam at the edge x= 10 cm	Beam at x= 30 cm	Beam at x= 50cm	Beam at x=70cm
50 GEV	Approximate -t byte $(Gev/c)^2$	0 - .11	.15-.5	.5 - 1.	1.-2.
	Approximate efficiency	50%	18%	12%	7%
	Events in the Diffraction peak	3.3×10^7	9.8×10^6	1.2×10^6	5×10^4
	Events for $M_x \geqslant 3$Gev when $m_c = m_a$; given for $\Delta M_x^2 = 1$ GeV^2	5.8×10^5	1.6×10^5	2.1×10^4	8×10^2
	Baryon exchange for $M_x \leqslant 1.4$ GeV	4.6×10^3	1.6×10^3	3×10^2	
100 GEV	Approximate -t byte $(Gev/c)^2$	0 -.44	.6 -2.0	2.- 4.	
	Approximate efficiency	50%	18%	12%	
	Events in the Diffraction peak	6.8×10^7	1.1×10^6	1.2×10^2	
	Events for $M_x \geqslant 3$ Gev when $m_c = m_a$; given for $\Delta M_x^2 = 1$ Gev^2	5.9×10^5	9.6×10^3	1	

Table III : Event rates calculated for 10^5 machine pulses (approximately six days of running) for a luminosity of $.4 \times 10^{30} cm^{-2} pulse^{-1}$. The same t dependence has been assumed for $M_x > 3$GeV and the diffraction peak.

F. Cerenkov Counters

The Cerenkov counters we plan to use are simple threshold counters. They will be constructed in modular units so as to accommodate the different configurations necessary to run the experiment at 50 and 100 GeV. Figure 14 shows the geometry, and Table IV shows the parameters for the two running configurations.

	COUNTER 1, π,K		COUNTER 2, π	
Parameters	50 GeV	100 GeV	50 GeV	100 GeV
length (m)	4	10	11	14
diameter (m)	.5	.5	.5	.5
pressure (Atm)	.6 Nigrogen	1.4 Helium	1.4 Helium	.3 Helium
θ_π (mrad)	18.6	9.6	9.6	4.8
n_π (photoelectron)	20	14	14	5
θ_K(mrad)	15.9	8.66		
n_K (photoelectrons)	15	11		

Table IV. Cerenkov counter parameters. We have estimated the number of photoelectrons by $n = A \cdot L\theta_c^2$ where $A = 150\ cm^{-1}$, L is the radiator length in cm. and θ_c is the Cerenkov angle in radians.

G. The Beam

The requirements we have placed on the beam so far are:

$$\Delta P/P = \pm .05\%$$
$$\pi^-/\text{spill} \approx 250K$$

These requirements are reasonable. The particle yields for the high resolution M6 beam of the meson laboratory are shown in Figures 15A and 15B. The heavy line in these figures represents a level of 250K particles per pulse. From these figures we conclude that we require less than 10^{12} protons on target to receive the required pion yields.

H. Comparison with other experiments

The main difference between our streamer chamber experiment and bubble chamber experiments which may overlap with our physics goals is the larger beam flux that the streamer chamber can utilize effectively. With a luminosity of ~ 10^{30} cm^{-2} $pulse^{-1}$, the streamer chamber yields a factor of 10^4 to 10^5 higher luminosities than the NAL bubble chambers. We use this increased luminosity a) to restrict the outgoing track to a given kind of particle and measure it with high resolution, and b) to explore regions which are inaccessible to the bubble chambers because of small cross sections.

The bubble chambers are quite inefficient even in the study of diffraction excitation at small momentum transfers. To study the diffractive bump in detail requires some 10^5 events. With an integrated cross section of 3mb this requires a 3.3×10^6 picture exposure of the 30" chamber. On the other hand, the streamer chamber is only limited by its cycling time, and can accomplish the same exposure in 2.5×10^4 pulses. In our proposed experiment we would also have particle identification and a high resolution measurement of the fast scattered track.

At large momentum transfers, or for particle exchange processes, the advantages of the streamer chamber become more pronounced.

Our proposed experiment has advantages over presently proposed wire chamber spectrometers in its ability to handle final states with complicated topologies. These topologies arise from the decay of strange particles and/or high multiplicity events. Furthermore by specifically designing an experiment to look at only one fast outgoing particle we achieve sufficient resolution to study events with one neutral particle in the final state. The streamer chamber provides an almost 4π detectors to observe the target fragments, with no geometrical biases arising from the trigger.

IV. IMPLEMENTATION

A. Personnel

The physicists submitting this proposal form the Birge Group at the Lawrence Berkeley Laboratory. If approved, the proposed experiment would become the primary future goal of the group. Our present commitments are:

1. Analysis of the diffraction dissociation experiment $\pi^{\pm}p \rightarrow \pi^{\pm} N^{*}$ at 14 GeV/c in collaboration with Caltech and SLAC (SLAC Bubble Chamber Experiment 25).
2. Analysis of the $\pi^{o}\pi^{o}$ interaction experiment $\pi^{+} + p \rightarrow p + \pi^{+} + n\pi^{o}$ at 4 GeV/c in collaboration with the Rutherford Laboratory and the Istituto di Fisica dell' Universita di Torino (Rutherford Track Sensitive Bubble Chamber Experiment).
3. Data collection (Fall, 1973) and analysis of the streamer chamber experiment to study $\pi^{-}p \rightarrow p + X$ (Bevatron Experiment #155).

We feel that participation of more physicists is desirable and necessary for the success of this project. We expect to collaborate with other physicists from LBL as well as other institutions, including NAL.

B. Costs

The main cost of the experiment is the streamer chamber and associated magnet. While our experiment could run successfully with a small streamer chamber, of approximate dimensions 1.5m x 1 m x .60m, we feel that a larger streamer chamber would be desirable as a general tool at NAL. We want to discuss the alternatives with NAL.

We expect NAL to provide all the magnets as listed in Table V,

while we hope to construct the streamer chamber and pulsing network at LBL with some financial support from NAL.

All the proportional chambers and related electronics, including the hard-wired arithmetic unit, will be constructed by LBL.

C. Machine Time Requirements

We estimate that we need some 5×10^5 pulses of the machine to accomplish our original goal. We will run at 50 GeV and 100 GeV with an incident π^- beam. Each energy will then be divided into three runs between transverse momenta of 0 and 1.5 GeV/c^2. Our group, or other groups, may be interested in extensions of the experiment to higher energies.

ITEM	PROVIDER	COST KILODOLLARS
High resolution beam $\frac{\Delta P}{P} < .1\%$	NAL	--
Streamer chamber magnet (minimum: 0.6m gap x 1m wide x 1.5m long, 30 kg.m.)	NAL	--
Compensator magnet (.05m gap x .01m wide x 1m long)	NAL	--
2 Bending magnets (.2m gap x .4m wide x 2m long; 40 kg.m; field uniformity .05%)	NAL	--
Streamer Chamber and associated trigger electronics	LBL with help from NAL	~200K
Proportional wire chambers	LBL	40K
Arithmetic unit	LBL	20K
Cerenkov Counters	LBL	5K
Small Data Logging Computer	LBL	--

TABLE V

REFERENCES

1. E. W. Anderson et al., Phys. Rev. Letters 16, 855 (1966).
2. For an extensive review see for example "Diffraction Dissociation", D. Leith, SLAC-PUB-1141.
3. Caltech-Berkeley-SLAC collaboration. See, for instance, LBL preprint 747.
4. Carnegie Mellon-Rochester-Northwestern collaboration. Some results were presented at the Washington meeting, April, 1973. APS Bulletin 18, 640 (1973).
5. Y. M. Antipov, et al., Physics Letters, 40B, 1(1972);
   Y. M. Antipov, et al., NAL Conference paper #442 (1972);
   G. Ascoli, NAL Conference paper #444 (1972).
6. For a summary of ISR and NAL results see M. Jacobs' "Diffraction Excitation" summary of ISR Discussion Meeting #5.
7. 300 GeV pp NAL-UCLA collaboration.
8. NAL Proposal #96.
9. E. W. Anderson et al., Phys. Rev. Letters 22, 1390 (1969).
10. M. Bishari, Physics Letters 38B, 312 (1971).
11. R. S. Larsen, SLAC-PUB-1160.
12. See, for example, D. J. Crennell et al., Phys. Rev. Letters 28, 643 (1972).

FIGURE 1: The Geometry of the Apparatus

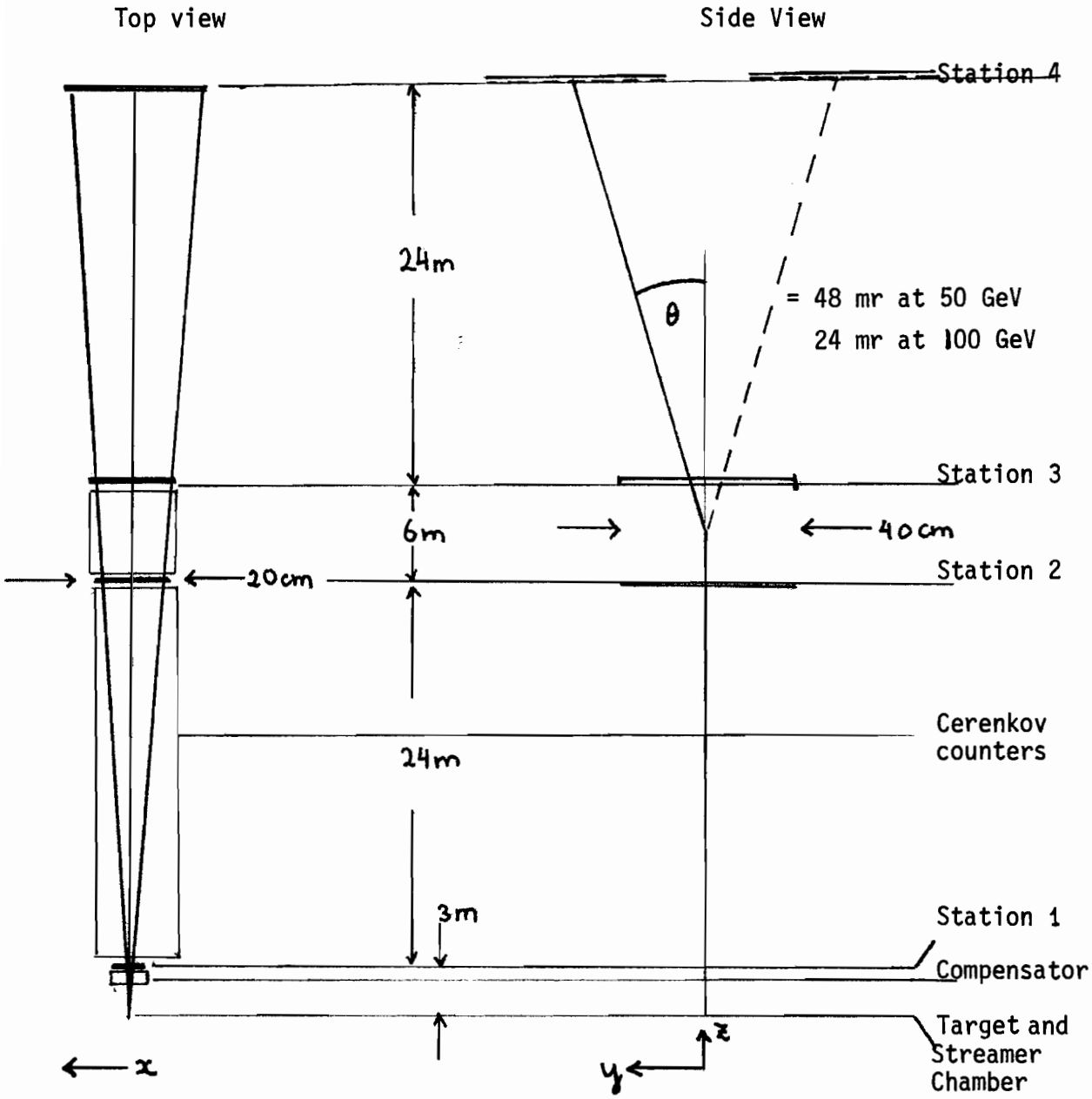

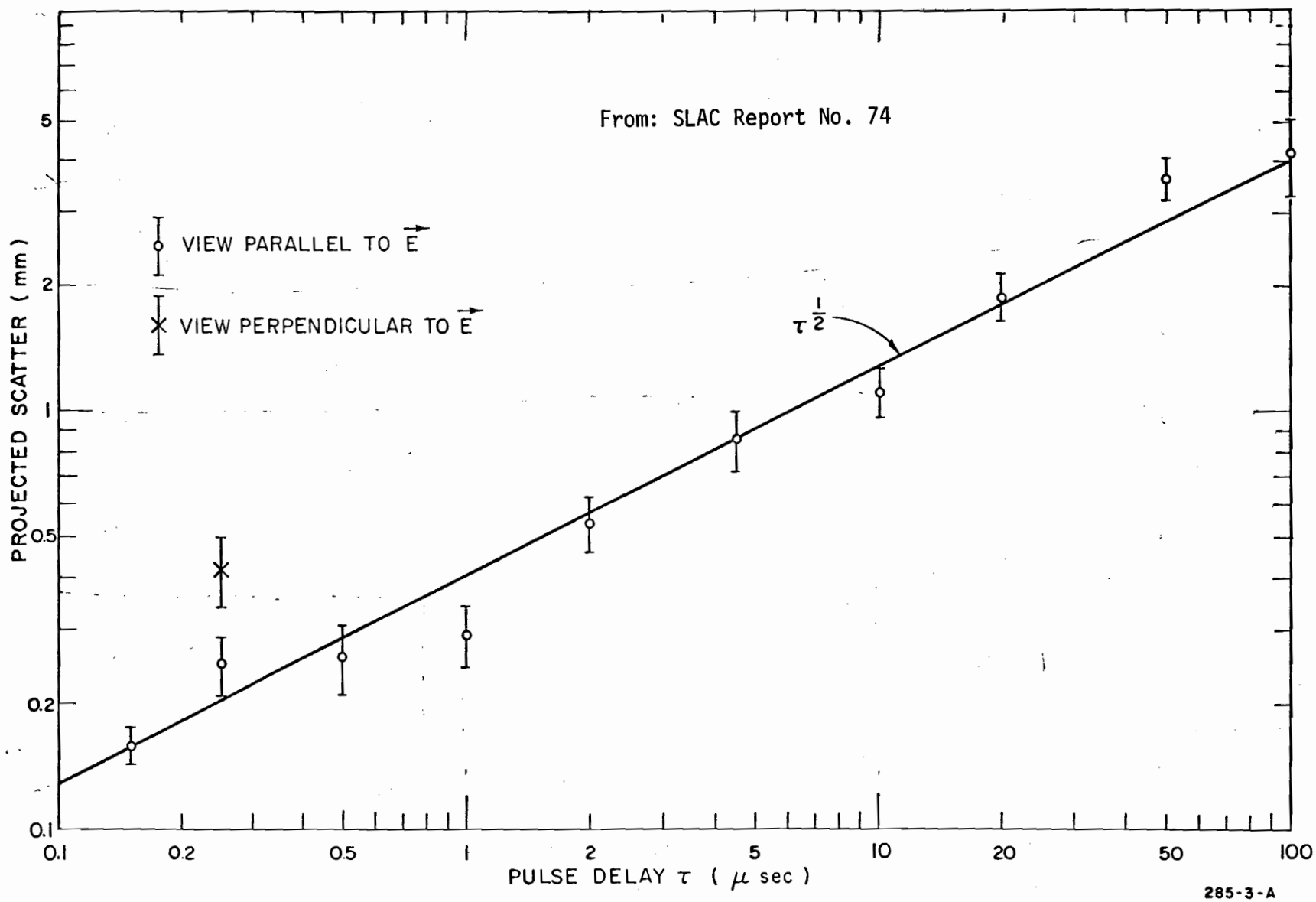

--Projected scatter of the diffused streamer track plotted as a function of the pulse delay τ in μsec. Essentially this figure indicates the accuracy with which the axis of a streamer track can be found with various pulse delays.

Figure 2

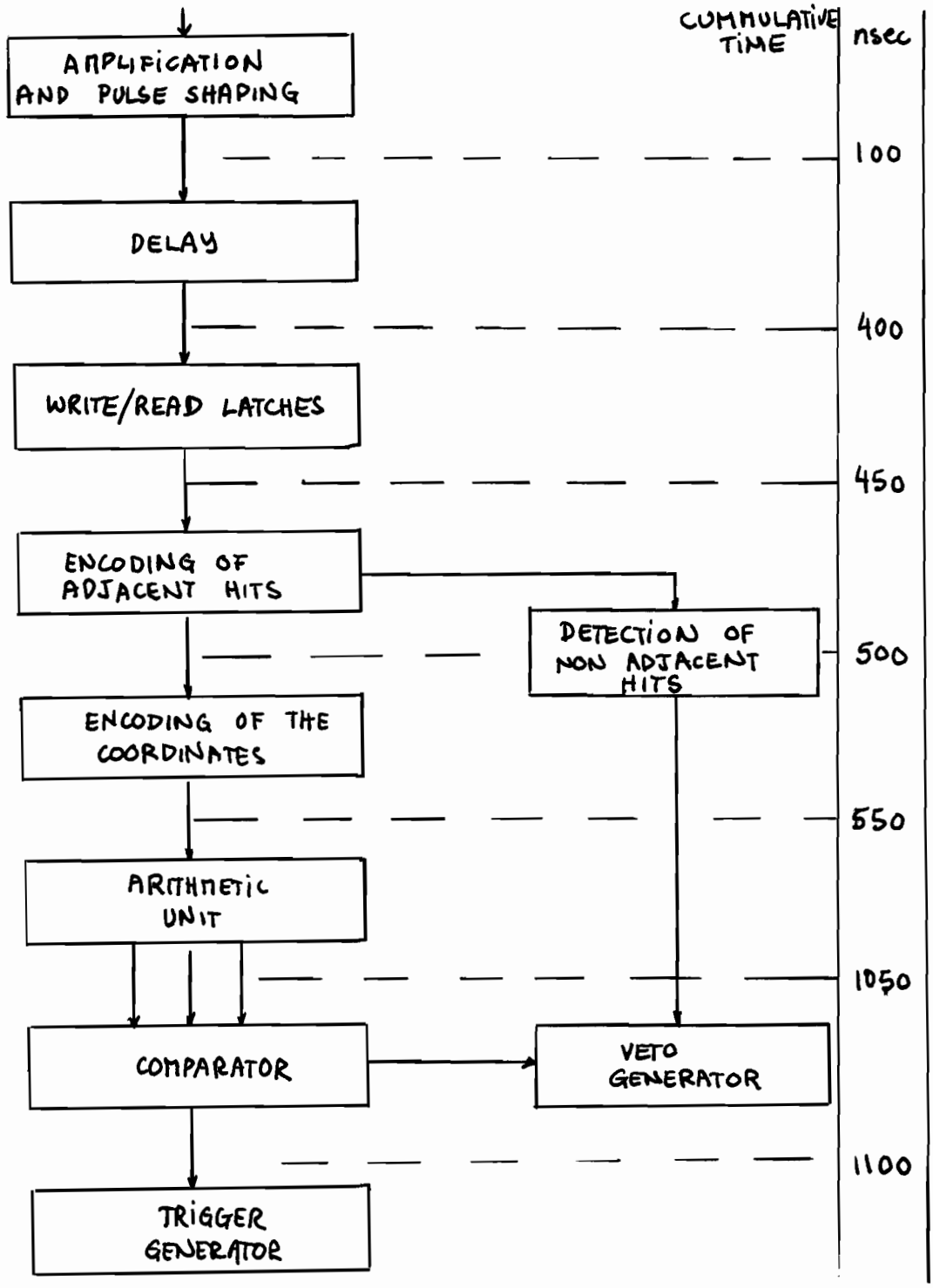

FIGURE 3: General Scheme for the Proportional Chamber Electronics

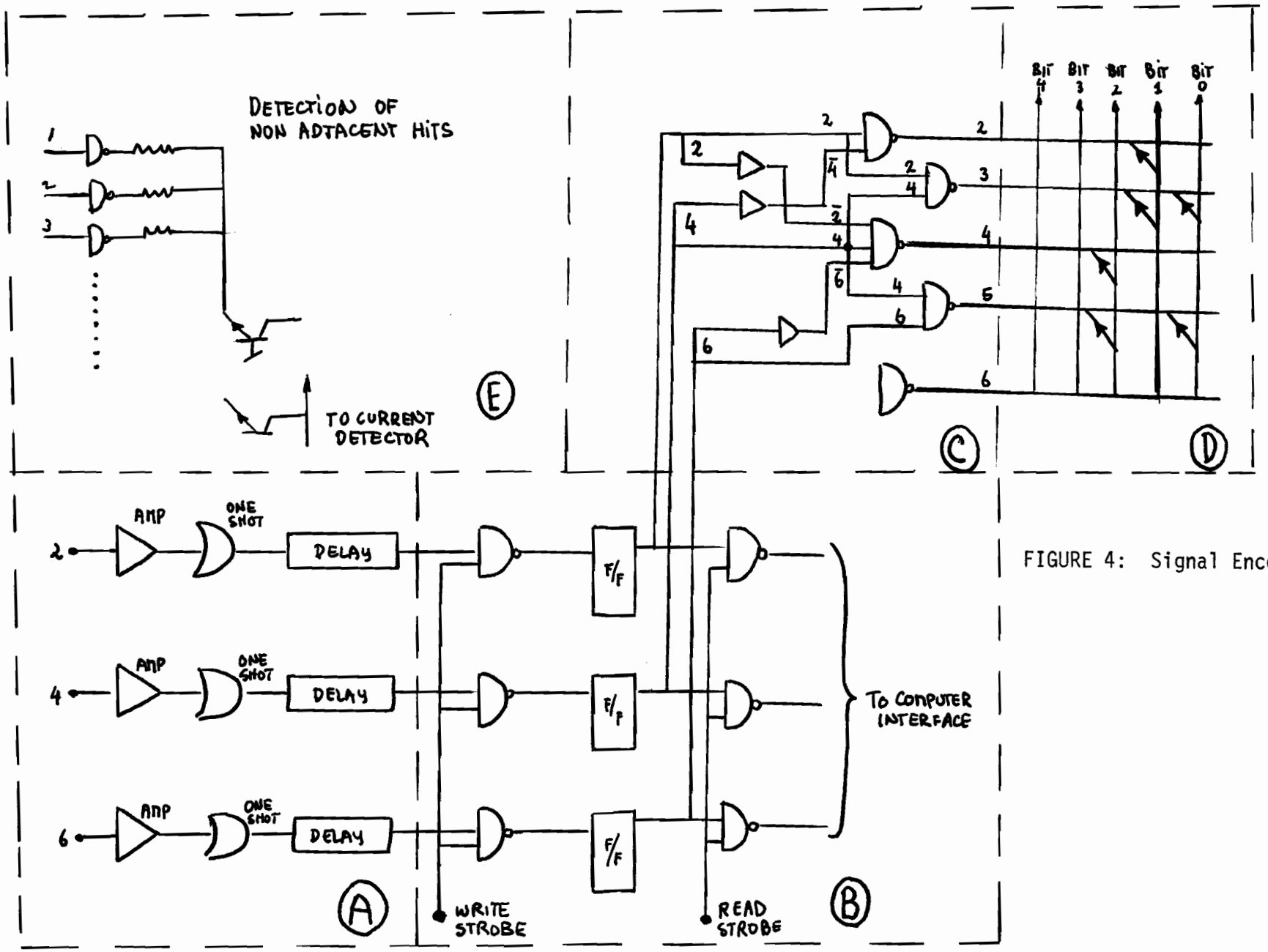

FIGURE 4: Signal Encoding

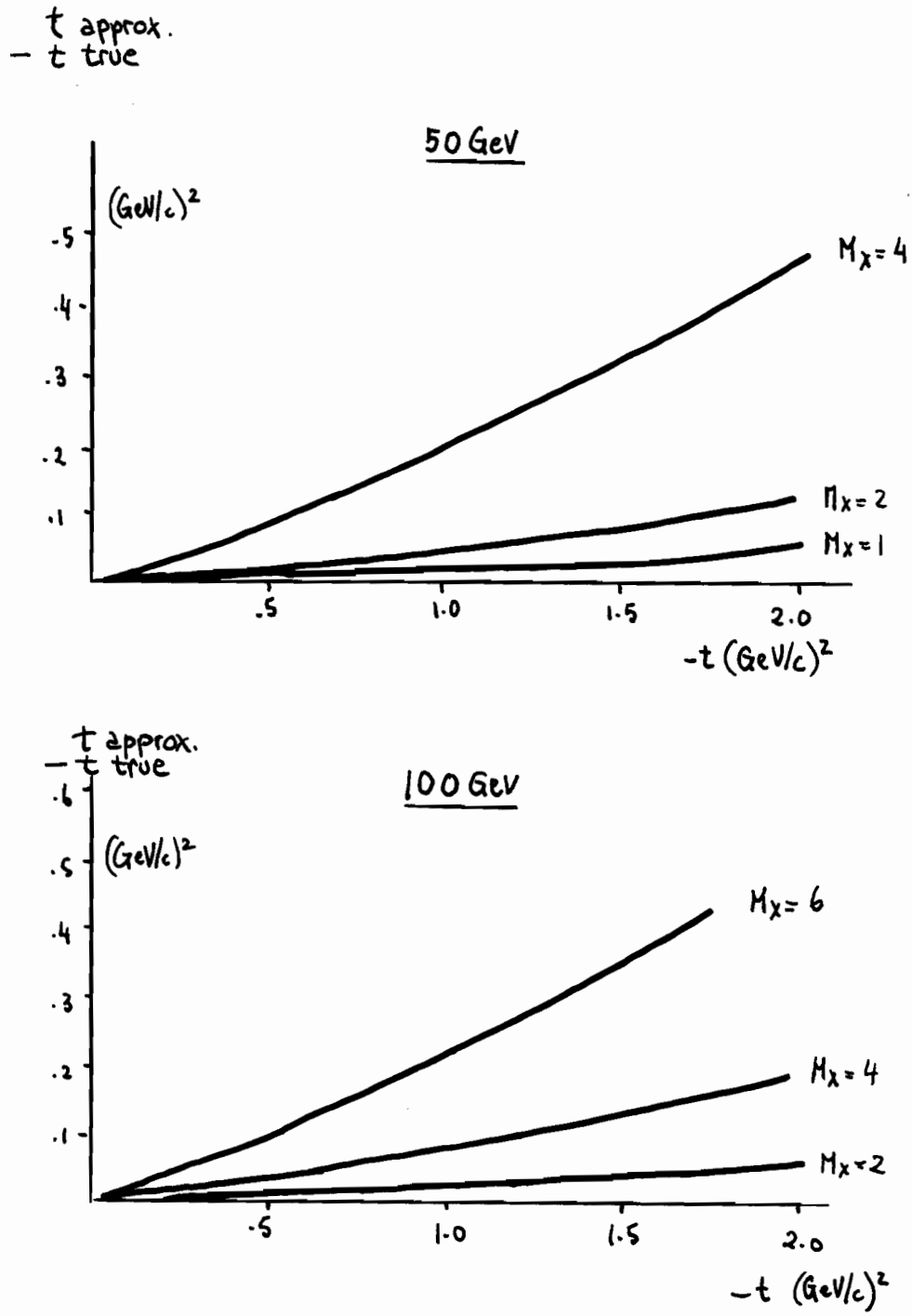

FIGURE 5: The t approximation used in the fast calculations

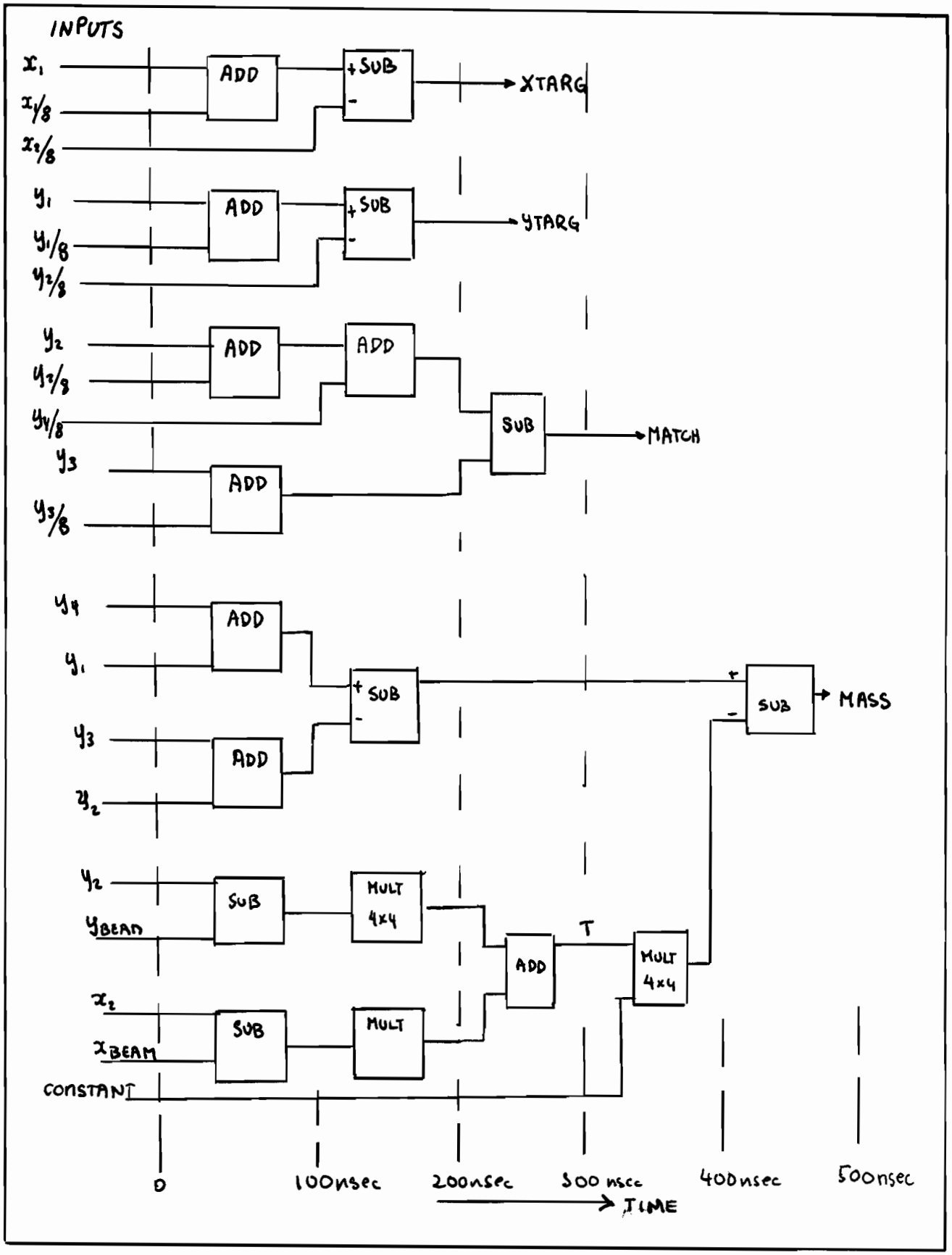

FIGURE 6: The Arithmetic Unit

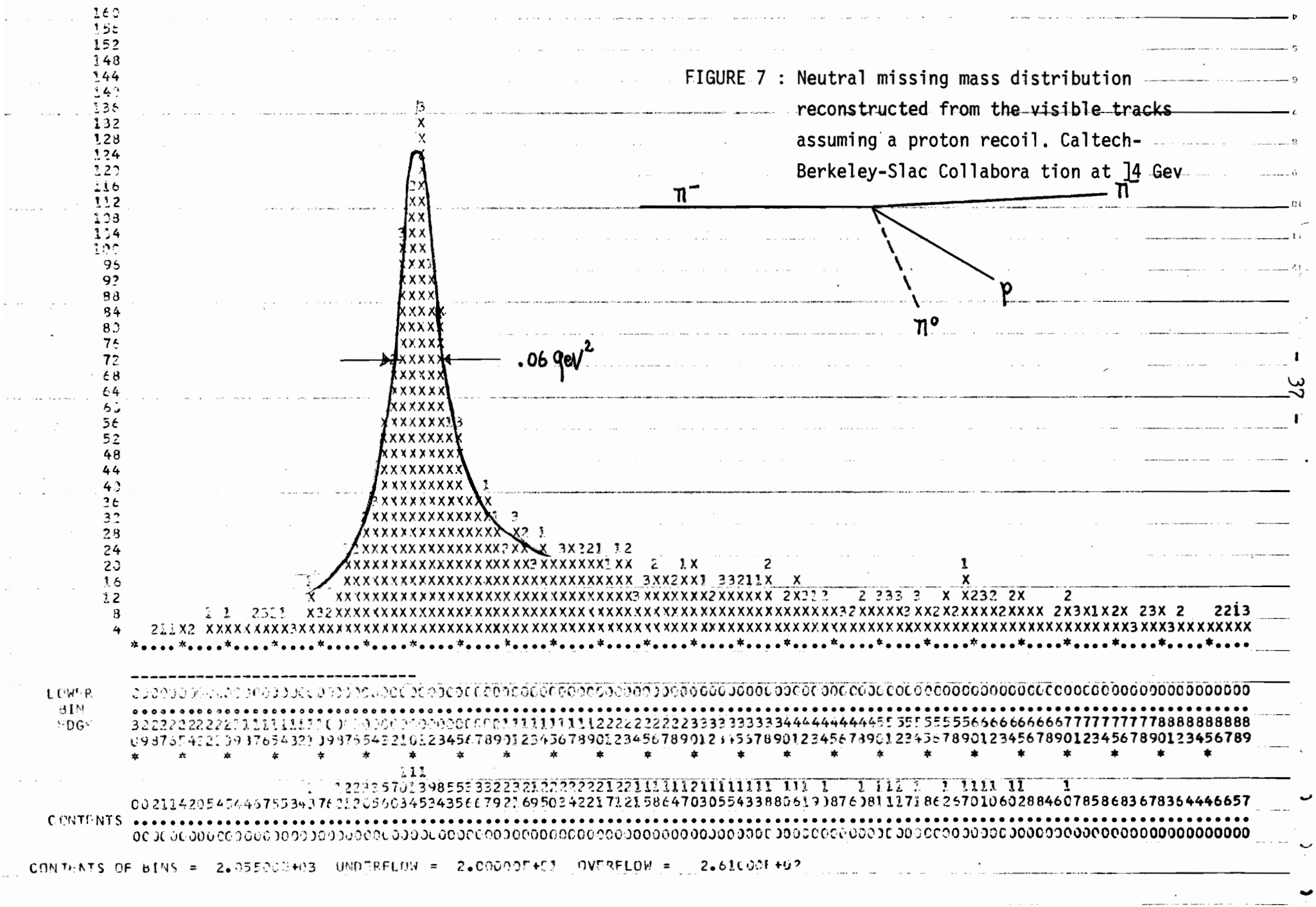

FIGURE 7 : Neutral missing mass distribution reconstructed from the visible tracks assuming a proton recoil. Caltech-Berkeley-Slac Collabora tion at 14 Gev

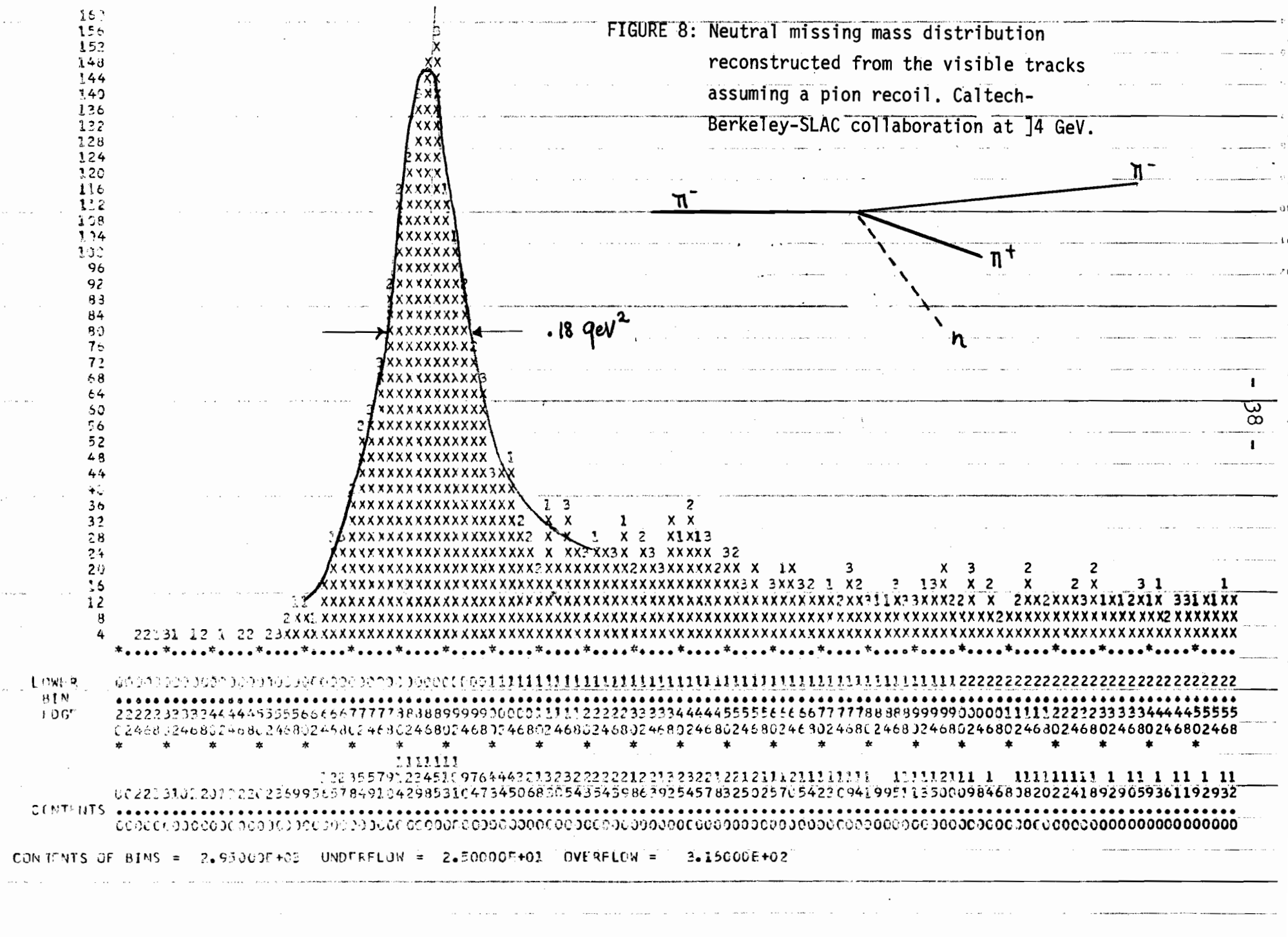

FIGURE 8: Neutral missing mass distribution reconstructed from the visible tracks assuming a pion recoil. Caltech-Berkeley-SLAC collaboration at]4 GeV.

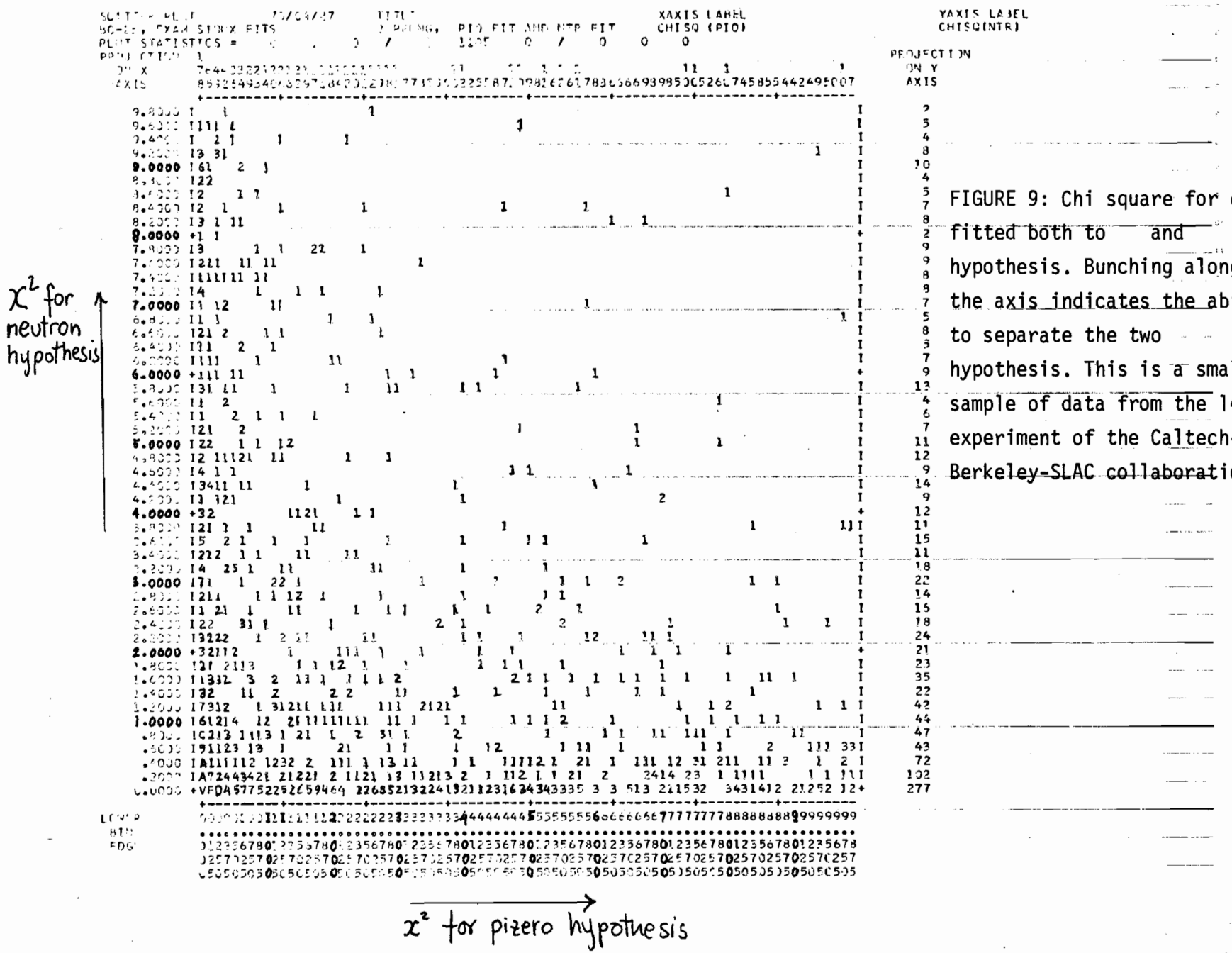

FIGURE 9: Chi square for events fitted both to and hypothesis. Bunching along the axis indicates the ability to separate the two hypothesis. This is a small sample of data from the 14 Gev experiment of the Caltech-Berkeley-SLAC collaboration

FIGURE 10 A: Images for fixed M_x and t at the spectrometer entrance, assuming the beam is centered

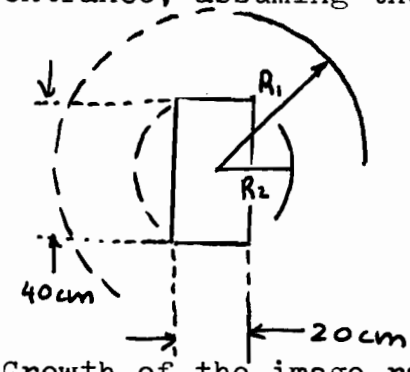

	t(50GeV)	t(100GeV)
for R_1	.5 $(GeV/c)^2$	2.0 $(GeV/c)^2$
for R_2	.1 $(GeV/c)^2$	.4 $(GeV/c)^2$

FIGURE 10 B: Growth of the image radius with momentum transfer for two masses; the beam is 50 GeV

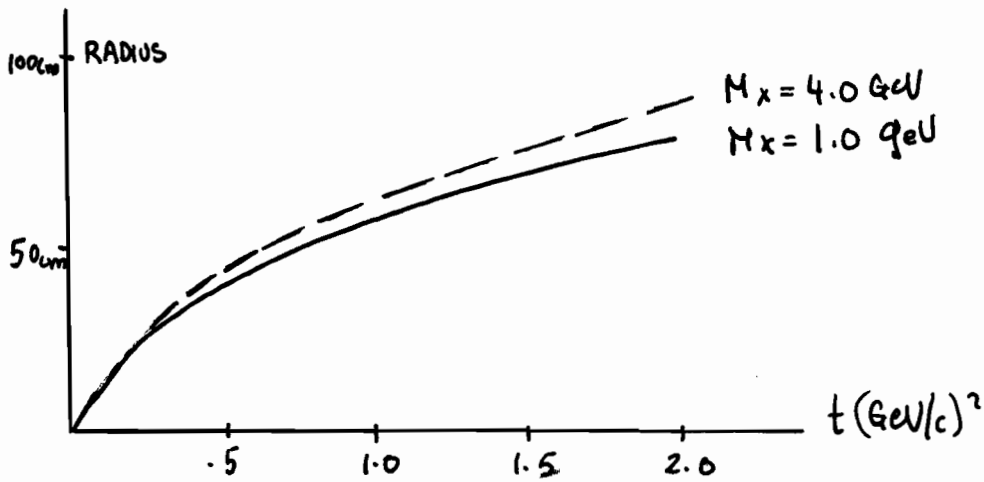

FiGURE 10 C: Dispersion due to the streamer chamber magnet at the entrance of the spectrometer.

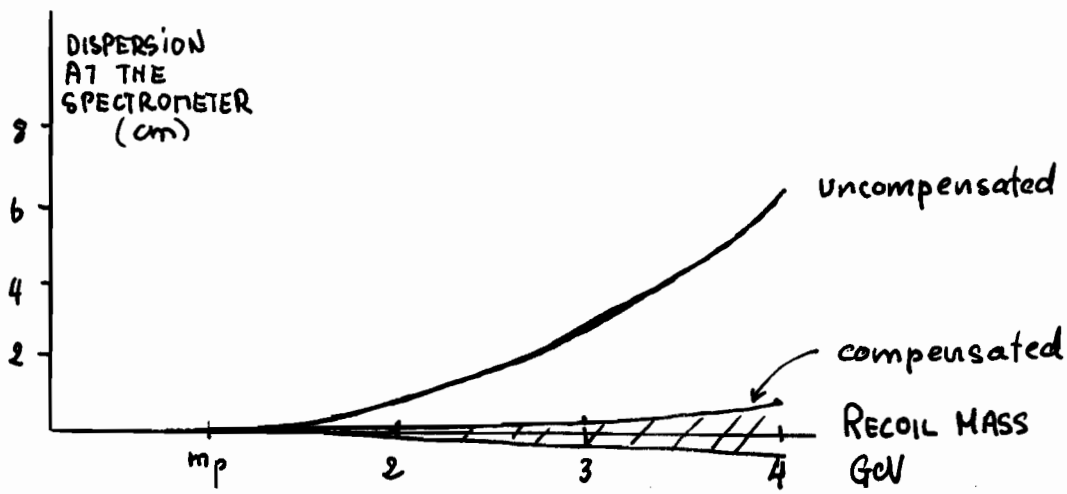

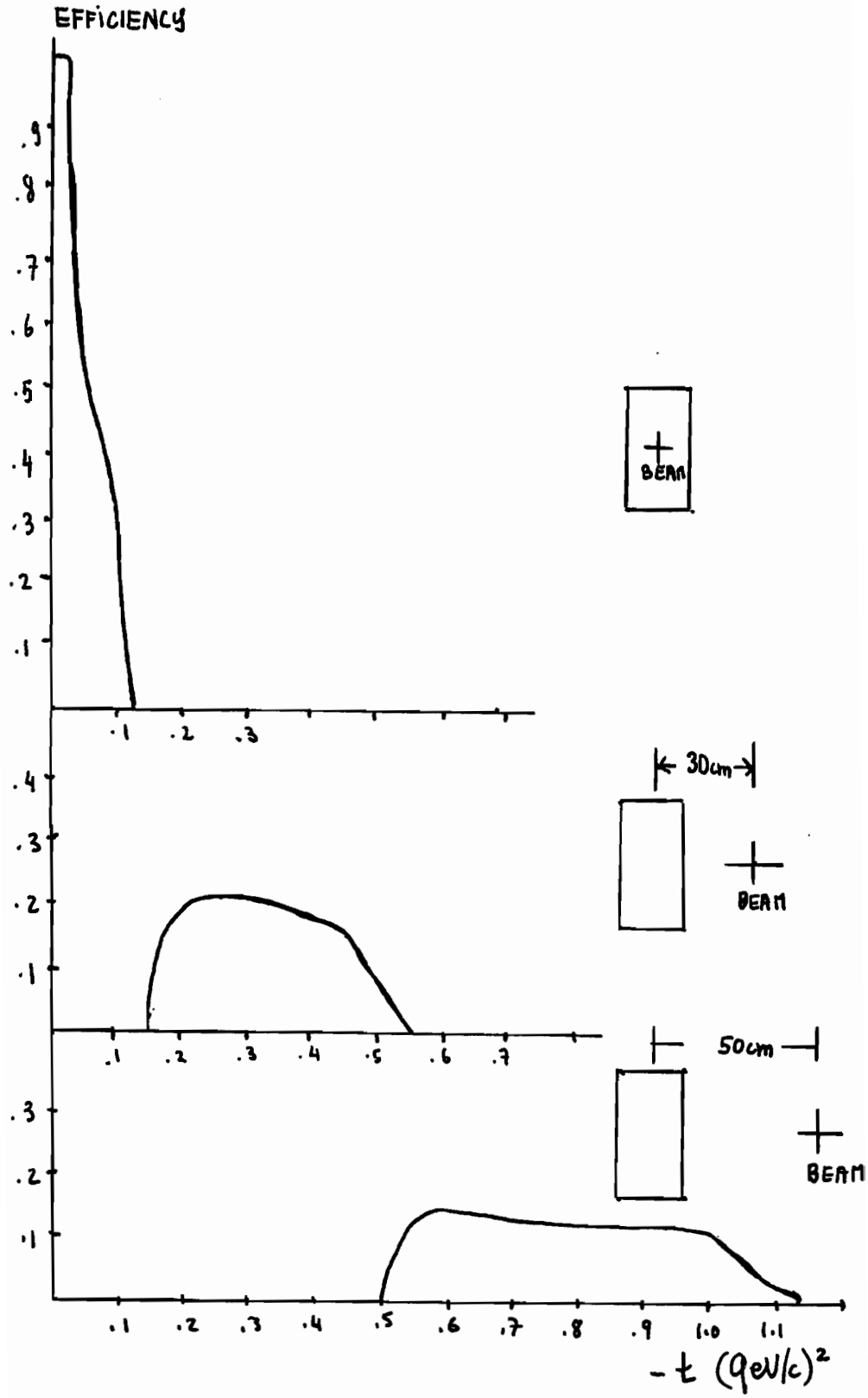

FIGURE 11: Momentum transfer acceptance as the spectrometer is displaced relative to the beam. Curves shown are for a 2 GeV recoil mass, with $P_{beam} = 50$ GeV

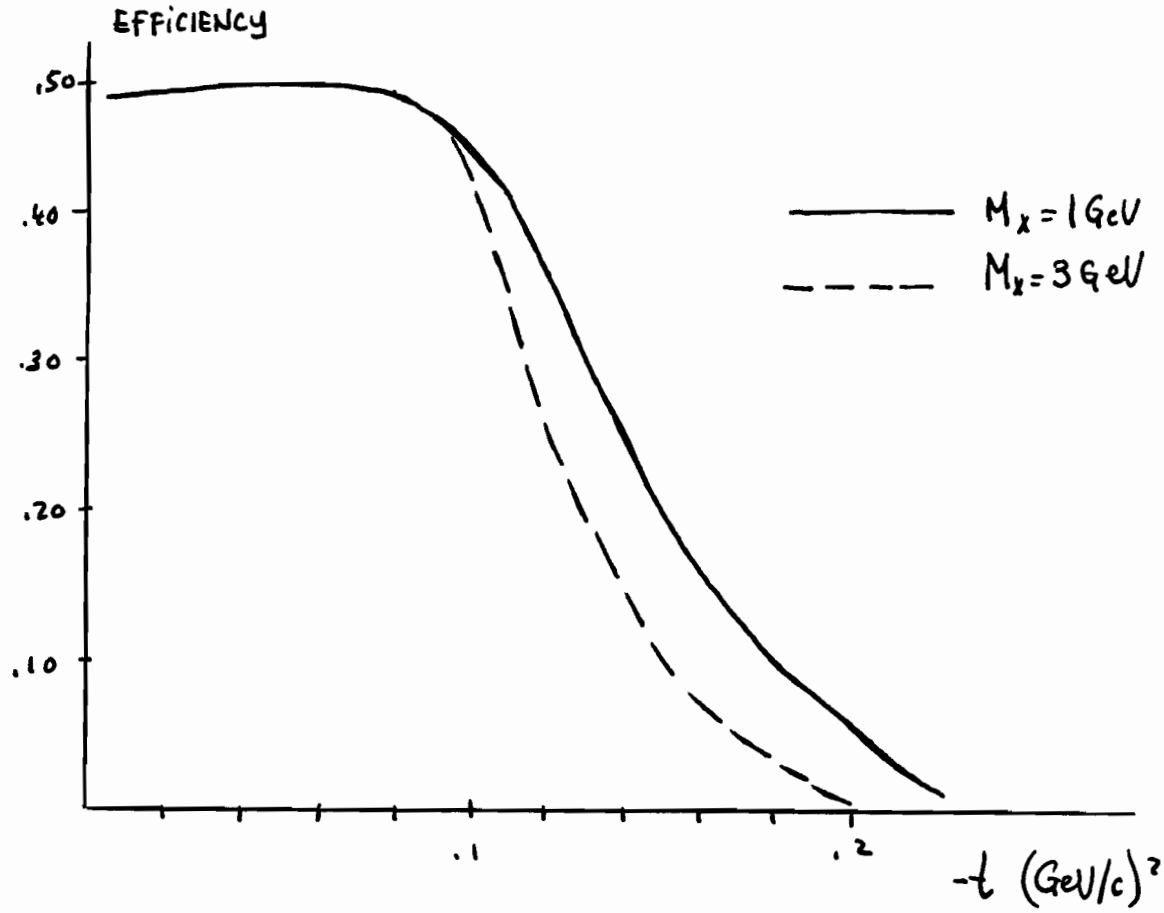

FIGURE 12 : Momentum transfer acceptance for $P_{beam} = 50$ GeV and the spectrometer set at the edge of the beam.

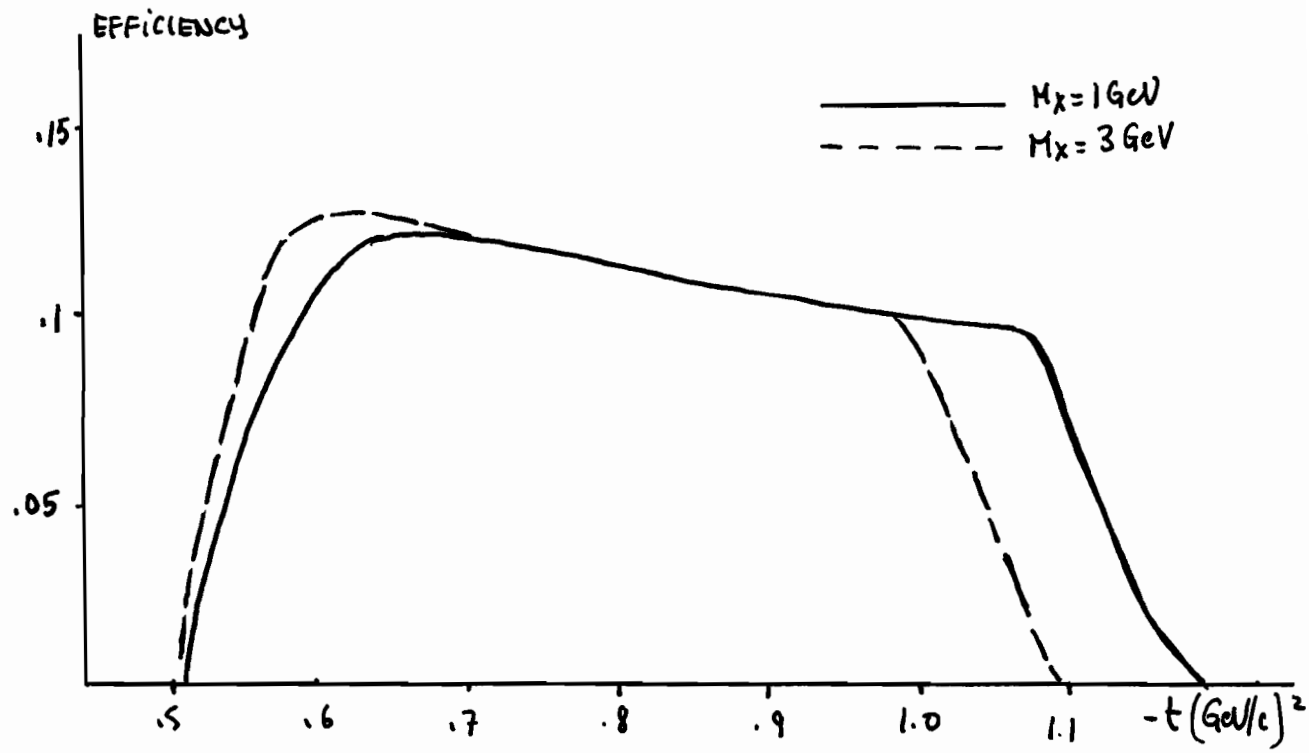

FIGURE 13 : Momentum transfer acceptance for $P_{beam} = 50$ Gev and the center of the spectrometer displaced 50 cm

FIGURE 14: Cerenkov counter configurations

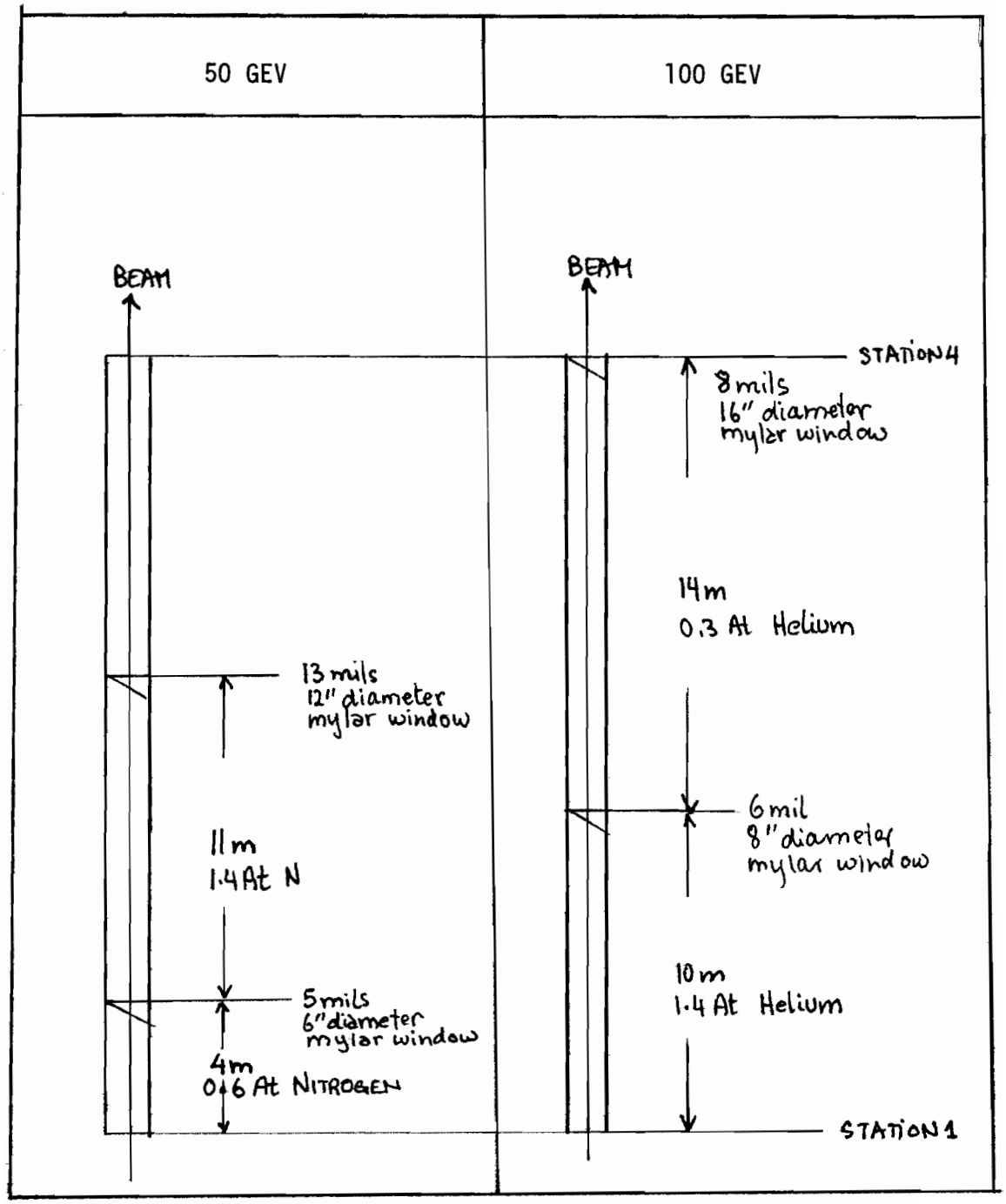

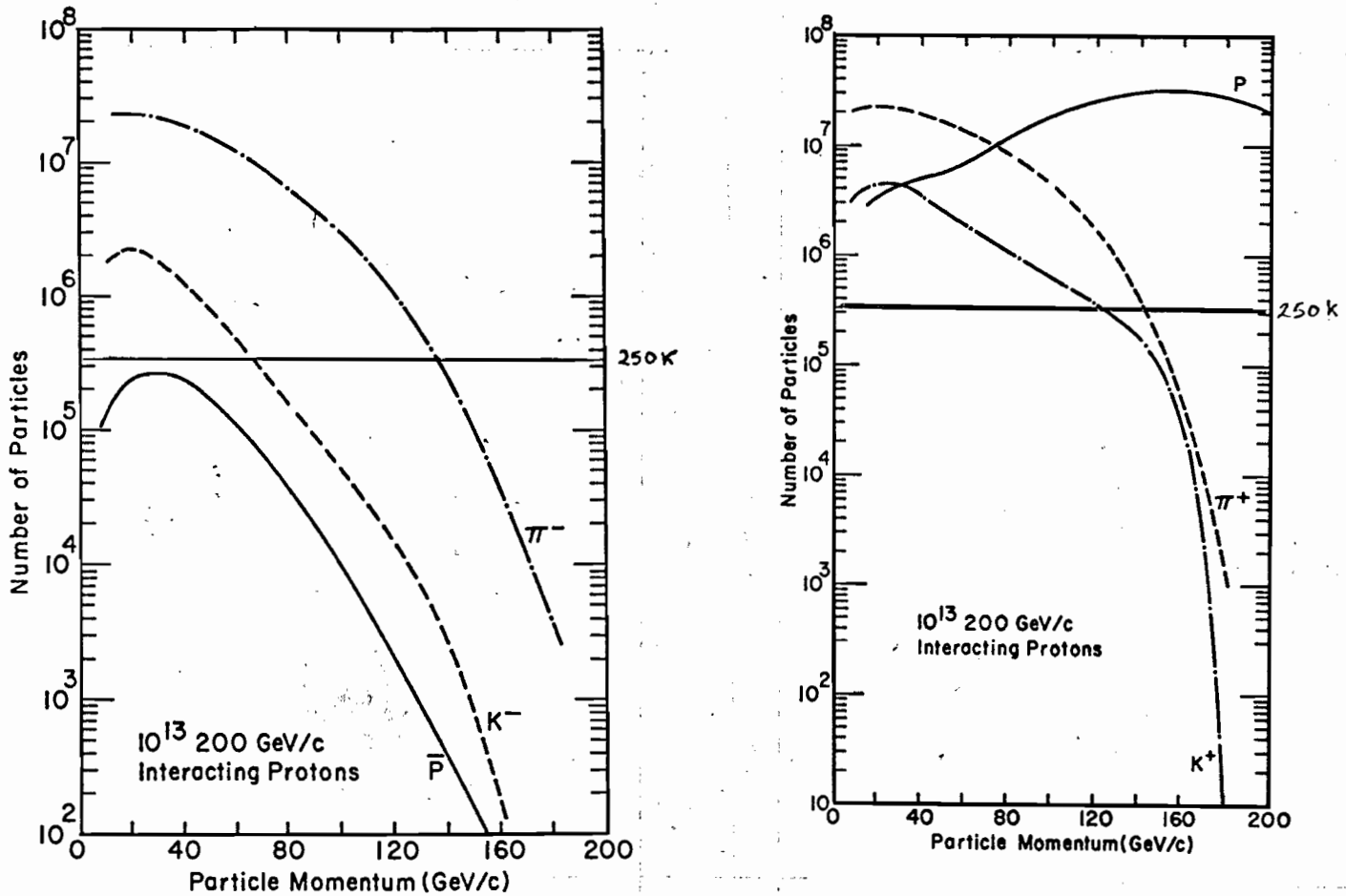

FIGURE 15: Estimated particle yields for the M6 beam, from J.R. Orr and A.L. Read's Meson Laboratory Preliminary Design Report 1971

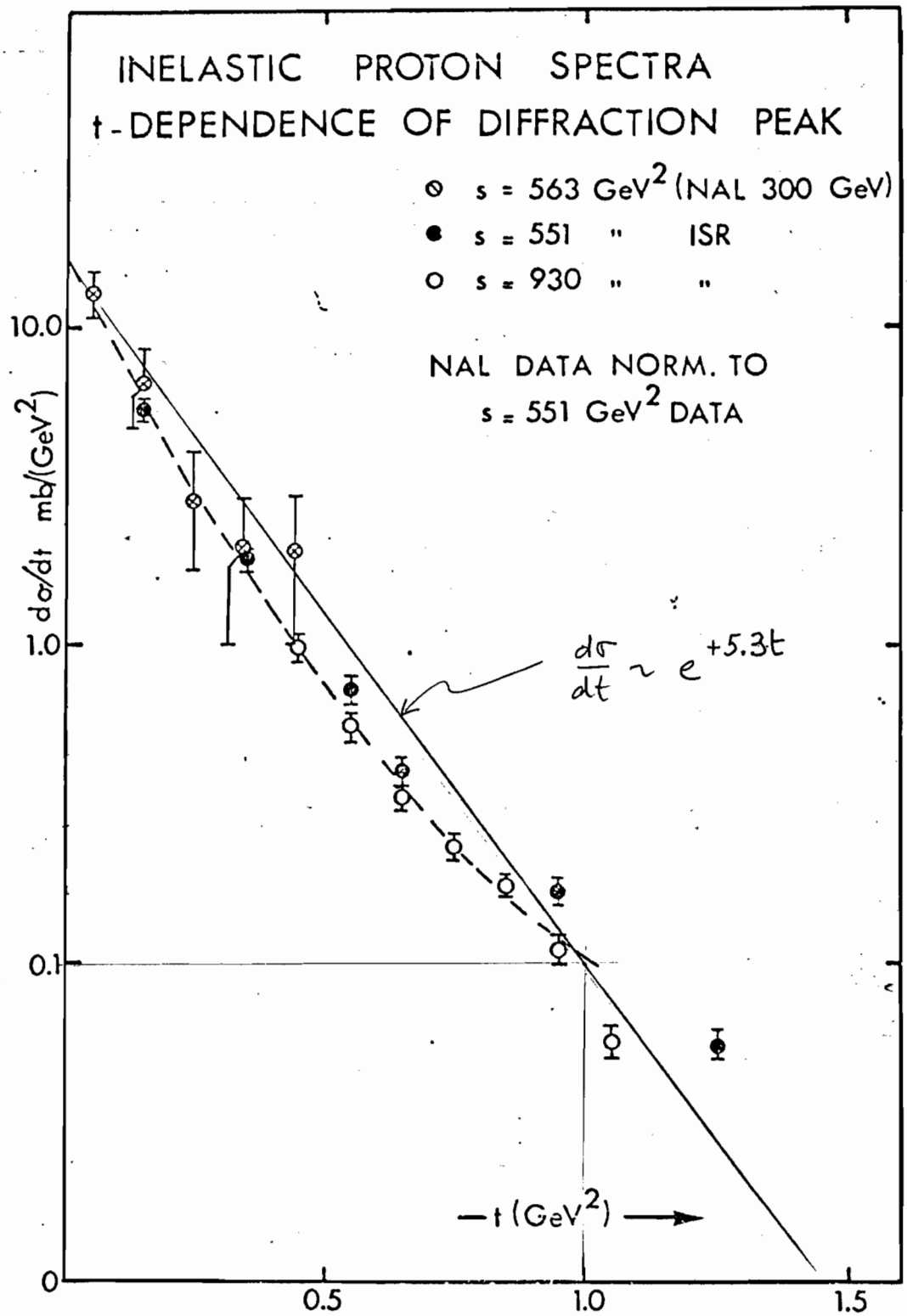

FIGURE 16 : The differential cross section for the integrated diffraction excitation "bump" . Data from the Cern-Holland-lancaster-Manchester collaboration